# Scalar-induced gravitational waves including isocurvature perturbations with lattice simulations

# Xiang-Xi Zeng $^{a,b}$

<sup>a</sup>Institute of Theoretical Physics, Chinese Academy of Sciences (CAS), Beijing 100190, China
 <sup>b</sup>School of Physical Sciences, University of Chinese Academy of Sciences (UCAS), Beijing 100049, China

E-mail: zengxiangxi@itp.ac.cn

Abstract. Scalar-induced gravitational waves (SIGWs) open a unique window into early-universe physics. While their generation from adiabatic perturbations has been extensively studied, the contribution from isocurvature perturbations remains poorly understood. In this work, we develop a lattice simulation framework to compute the stochastic gravitational wave background from both pure isocurvature and mixed initial conditions. Our numerical results show excellent agreement with semi-analytical predictions in the pure isocurvature case. We further analyze multi-peak structures under general initial conditions and find that they closely match those produced in purely adiabatic scenarios. Additionally, we examine SIGWs in early matter-dominated eras, revealing that the peak amplitude and spectral slope are sensitive to the microphysical properties of the dominant field, such as the primordial black hole mass, abundance, or soliton decay rate. This study establishes lattice simulations as a robust tool for predicting SIGW spectra from complex primordial perturbations, with important implications for interpreting current and future gravitational wave observations.

#### Contents

1	Introduction	1
2	Evolution of curvature and isocurvature perturbations	2
	2.1 Equations of motion	3
	2.2 The initial conditions	4
3	Simulation results without energy transfer	5
	3.1 Comparing with the semi-analytical predictions	(
	3.2 The peak structures of general initial conditions	(
4	Simulation results with energy transfer	7
	4.1 SIGW from eMD isocurvature	7
	4.2 SIGW from general initial conditions	11
5	Discussion and conclusions	11
$\mathbf{A}$	Semi-analytical formulas in isocurvature case	13

## 1 Introduction

A series of recent results from Pulsar Timing Array (PTA) collaborations (NANOGrav [1], EPTA [2], PPTA [3], and CPTA [4]) have brought us to the era of detecting a stochastic gravitational wave background (SGWB). The upcoming of advanced gravitational wave detectors, from space-based missions like LISA [5], Taiji [6, 7], TianQin [8] as well as the more advanced DECIGO [9] and BBO [10] to future ground-based facilities such as Einstein Telescope (ET) [11] and Cosmic Explorer (CE) [12]), will open a window onto a landscape of SGWBs encoding a wealth of new physics (see Refs. [13–15] for reviews). Beyond astrophysical sources, the SGWB offers a unique probe of the early universe, potentially encoding information from epochs far beyond the reach of traditional cosmic microwave background (CMB) observations. Among the most promising mechanisms for generating such a background are scalar-induced gravitational waves (SIGWs)(see Ref. [16] for a review), which are produced when primordial scalar perturbations re-enter the horizon and source tensor fluctuations through second-order gravitational interactions [17–21].

The properties of SIGWs are intimately tied to the nature of the primordial perturbations. While the majority of studies have focused on adiabatic perturbations [22–26], consistent with the models of single field inflation and strongly constrained by CMB observations [27–29], another fundamental class, isocurvature perturbations [30–34], remains a compelling and less explored possibility (see Ref. [35] for a review). Isocurvature modes, characterizing relative density contrasts between different cosmological components (e.g., radiation and dark matter), are a generic prediction of many multi-field inflation models [36–40], phase transition [41] and could be associated with the formation of primordial black holes (PBHs) [42–47] or other exotic non-topological relics like Q-balls [48, 49]. Crucially, isocurvature perturbations, particularly those of Poissonian origin such as from PBHs, are

inherently large, reaching amplitudes of O(1) [43, 44]. Consequently, they can generate a substantial SIGW signal and must be carefully accounted for.

The exact semi-analytical formalism for isocurvature-induced SIGWs was first given in Ref. [50], which is strictly valid only under the condition that the relevant perturbation modes enter the horizon long before matter-radiation equality, while the complexity escalates significantly for mixed initial conditions (with both adiabatic and isocurvature perturbations). In contrast, lattice simulations offer a robust alternative, with an intrinsic advantage in accurately capturing effects from non-Gaussianity. While this method has previously been applied exclusively to adiabatic fluctuations [51], we systematically extend it in this work to incorporate isocurvature perturbations and mixed initial conditions.

An early matter-dominated (eMD) epoch represents another compelling scenario [52]. During eMD, the gravitational potential is stabilized, leading to a significant enhancement of SIGWs [53, 54]. A critical factor is the transition timescale out of eMD: a fast transition triggers a resonant amplification (poltergeist mechanism) [54], while a slow transition suppresses the signal [55–57]. Despite existing numerical work on adiabatic initial conditions [55–57], little attention has been paid to the numerical investigation of isocurvature perturbations. For this purpose, we adopt the lattice simulation method, which is well-suited to this problem.

The remainder of this paper is structured as follows. Section 2 is devoted to the theoretical formalism for cosmological perturbations incorporating isocurvature modes, along with a description of the numerical methodology. A comprehensive analysis comparing lattice simulations with semi-analytical results and the multi-peak phenomena under general initial conditions is presented in Section 3. Section 4 investigates the implications of this method within various eMD era scenarios. The paper concludes in Section 5 with a summary of our results and a discussion of prospective future work. We work in reduced Planck units where  $c = \hbar = 1$  and  $M_{\rm pl} = (8\pi G)^{-1/2} = 1$ . All our simulations employ a lattice size of N = 256, with the initial time set to  $\tau_i = 4/N$ .

# 2 Evolution of curvature and isocurvature perturbations

Isocurvature perturbations are generated by entropy perturbations, which necessitate the presence of multiple constituents in the universe [30–32]. Accordingly, our analysis requires at least two distinct fluids. Here, as a typical example, we assume the universe is composed of radiation and non-relativistic matter, and generalize to other kinds of fluids similar to Ref. [58] or the cases with more than two components should be straightforward. The energy-momentum tensors of the radiation and the matter are, respectively, given by

$$T_{(r)\mu\nu} = (\rho_{(r)} + p_{(r)})u_{(r)\mu}u_{(r)\nu} + p_{(r)}g_{\mu\nu}, \tag{2.1}$$

$$T_{(m)\mu\nu} = \rho_{(m)} u_{(m)\mu} u_{(m)\nu}, \tag{2.2}$$

where  $g_{\mu\nu}$  is the metric,  $\rho$  denotes the energy density, p is the pressure, and  $u_{\mu}$  is the four-velocity of fluid. Hereafter, we mainly follow the conventions established in Ref. [35], and the metric in Newtonian gauge is expressed as

$$ds^{2} = a^{2}(\tau) \left[ -(1 + 2\Psi)d\tau^{2} + ((1 + 2\Phi)\delta_{ij} + h_{ij}) dx^{i} dx^{j} \right],$$
(2.3)

where a is the scale factor,  $\tau$  is the conformal time,  $\Psi$  and  $\Phi$  denotes the scalar potential, and  $h_{ij}$  are the tensor perturbations. Given the definition of  $h_{ij}$ , the energy spectrum of GWs is

expressed as [59]

$$\Omega_{\rm GW}(\tau) = \frac{\rho_{\rm GW}(\tau)}{\rho_c(\tau)} = \frac{1}{12\mathcal{H}^2} \langle h'_{ij} h'_{ij} \rangle, \tag{2.4}$$

with  $\rho_c(\tau)$  denoting the critical energy density at time  $\tau$  and angle brackets describing a volume average.

# 2.1 Equations of motion

At the level of background, one has the Friedmann equations

$$3\mathcal{H}^2 = a^2(\rho_{(m)} + \rho_{(r)}),\tag{2.5}$$

$$3(\mathcal{H}^2 + 2\mathcal{H}') = -a^2 \rho_{(r)}, \tag{2.6}$$

where  $\mathcal{H}$  is the conformal Hubble parameter, defined as a'/a, with the prime denoting differentiation with respect to conformal time  $\tau$ . For the energy-momentum conservation equations, an energy transfer Q between components is typically accounted for

$$\nabla_{\mu} T^{(m)\mu\nu} = -Q^{\nu},\tag{2.7}$$

$$\nabla_{\mu} T^{(r)\mu\nu} = Q^{\nu}. \tag{2.8}$$

Given our focus on the early matter-dominated era (eMD), we accordingly assume that  $Q^{\mu}$  originates entirely from the matter sector, and define it as

$$Q^{\mu} \equiv Q u^{\mu}_{(m)}. \tag{2.9}$$

Hence, the above equations at the zeroth order arrive at

$$\rho'_{(m)} + 3\mathcal{H}\rho_{(m)} = -aQ, \tag{2.10}$$

$$\rho'_{(r)} + 4\mathcal{H}\rho_{(r)} = aQ. \tag{2.11}$$

At first order in perturbation theory, we neglect the transverse modes for  $u_{(m)}, u_{(r)}$  and define  $u_{(m),i} \equiv a\partial_i v_{(m)}$  and  $u_{(r),i} \equiv a\partial_i v_{(r)}$ . Assuming the absence of anisotropic stress,  $\Phi = -\Psi$  follows. To derive the perturbative equations, we have used the **xPand** [60] to perform the calculation. The perturbed Einstein equations are given by

$$6\mathcal{H}\Phi' + 6\mathcal{H}^2\Phi - 2\Delta\Phi = a^2(\delta\rho_{(m)} + \delta\rho_{(r)}) \equiv a^2\delta\rho, \tag{2.12}$$

$$\Phi' + \mathcal{H}\Phi = \frac{1}{2}a^2 \left(\rho_{(m)}v_{(m)} + \frac{4}{3}\rho_{(r)}v_{(r)}\right) \equiv \frac{1}{2}a^2\rho V, \tag{2.13}$$

$$\Phi'' + 3\mathcal{H}\Phi' + (\mathcal{H}^2 + 2\mathcal{H}')\Phi = -\frac{1}{6}a^2\delta\rho_{(r)},$$
(2.14)

while the energy-momentum conservation yields

$$\delta \rho'_{(m)} + 3\mathcal{H}\delta \rho_{(m)} + \rho_{(m)}(3\Phi' + \Delta v_{(m)}) = -a\delta Q + a\Phi Q,$$
 (2.15)

$$\delta \rho'_{(r)} + 4\mathcal{H}\delta \rho_{(r)} + \frac{4}{3}\rho_{(r)}(3\Phi' + \Delta v_{(r)}) = a\delta Q - a\Phi Q,$$
 (2.16)

$$v'_{(m)} + \mathcal{H}v_{(m)} - \Phi = 0, \tag{2.17}$$

$$v'_{(r)} + \frac{1}{4} \frac{\delta \rho_{(r)}}{\rho_{(r)}} - \Phi = \frac{aQ}{\rho_{(r)}} \left( \frac{3}{4} v_{(m)} - v_{(r)} \right). \tag{2.18}$$

At second order in perturbation theory, one can find the equations of tensor modes

$$h_{ij}'' + 2\mathcal{H}h_{ij}' - \Delta h_{ij} = T_{ij}^{lm} S_{lm}, \tag{2.19}$$

with the source term

$$S_{ij} = 4\partial_i \Phi \partial_j \Phi + 2a^2 \left( \rho_{(m)} \partial_i v_{(m)} \partial_j v_{(m)} + \frac{4}{3} \rho_{(r)} \partial_i v_{(r)} \partial_j v_{(r)} \right), \tag{2.20}$$

and  $T_{ij}^{lm}$  is the transverse-traceless projection operator defined by

$$T_{ijlm} = P_{il}P_{jm} - \frac{1}{2}P_{ij}P_{lm}, \quad P_{ij} = \delta_{ij} - \frac{\partial_i\partial_j}{\partial^2}.$$
 (2.21)

In our simulation, the scale factor  $a(\tau)$  and conformal Hubble parameter  $\mathcal{H}$  are evolved using Eq. (2.5), while Eq. (2.6) determines  $\mathcal{H}'$ . The energy densities  $\rho_{(m)}$  and  $\rho_{(r)}$  are advanced via Eqs. (2.10) and (2.11), respectively. For the perturbative sector, Eqs. (2.14), (2.15), (2.16), (2.17), (2.18), and (2.19) govern the evolution of  $\Phi$ ,  $\delta\rho_{(m)}$ ,  $\delta\rho_{(r)}$ ,  $v_{(m)}$ ,  $v_{(r)}$  and  $h_{ij}$ , respectively. Simulations are performed in a comoving cubic box with periodic boundary conditions, following Ref. [51]. Spatial derivatives are computed using a Fourier pseudospectral method, and time integration is handled by a fourth-order Runge-Kutta scheme.

#### 2.2 The initial conditions

It's conventional to define the isocurvature perturbation S to describe the behavior of relative density fluctuations between different components

$$S \equiv \frac{\delta \rho_{(m)}}{\rho_{(m)}} - \frac{\delta \rho_{(r)}}{\rho_{(r)} + p_{(r)}} = \frac{\delta \rho_{(m)}}{\rho_{(m)}} - \frac{3}{4} \frac{\delta \rho_{(r)}}{\rho_{(r)}}, \tag{2.22}$$

where we used  $p_{(r)} = 1/3\rho_{(r)}$ . From the equations of motion in Subsection 2.1, the evolution equation for S can be derived by

$$S' = -\Delta V_{\text{rel}} - a(\delta Q - Q\Phi) \frac{3}{4} \frac{\rho_{(m)} + 4\rho_{(r)}/3}{\rho_{(m)}\rho_{(r)}} + aQ\left(\frac{\delta \rho_{(m)}}{\rho_{(m)}^2} + \frac{3}{4} \frac{\delta \rho_{(r)}}{\rho_{(r)}^2}\right)$$
(2.23)

with  $V_{\rm rel} \equiv v_{(m)} - v_{(r)}$  denoting the relative velocity, and the equations of  $V_{\rm rel}$  and  $\Phi$  can also be obtained and rewritten as

$$V_{\rm rel}' + 3c_s^2 \mathcal{H} V_{\rm rel} + \frac{3}{2a^2 \rho_{(r)}} c_s^2 \Delta \Phi + \frac{3\rho_{(m)}}{4\rho_{(r)}} c_s^2 S - \frac{aQ}{4\rho_{(r)}} \frac{\rho V - 4(\rho_{(m)} + \rho_{(r)})V_{\rm rel}}{\rho_{(m)} + 4\rho_{(r)}/3} = 0, \quad (2.24)$$

$$\Phi'' + 3\mathcal{H}(1 + c_s^2)\Phi' + (\mathcal{H}^2(1 + 3c_s^2) + 2\mathcal{H}')\Phi - c_s^2\Delta\Phi = \frac{a^2}{2}\rho_{(m)}c_s^2S,$$
(2.25)

where the sound speed is defined as

$$c_s^2 = \frac{1}{3} \left( 1 + \frac{3\rho_{(m)}}{4\rho_{(r)}} \right)^{-1} = \frac{4}{9} \frac{\rho_{(r)}}{\rho_{(m)} + 4\rho_{(r)}/3}.$$
 (2.26)

When there is no energy transfer, namely,  $Q = \delta Q = 0$ , the scale factor has an analytical form

$$\frac{a(\tau)}{a_{\text{eq}}} = 2\left(\frac{\tau}{\tau_*}\right) + \left(\frac{\tau}{\tau_*}\right)^2,\tag{2.27}$$

where  $a_{\rm eq}$  denotes  $a(\tau_{\rm eq})$  at the time of matter-radiation equality, and  $\tau_{\rm eq} = (\sqrt{2} - 1)\tau_*$ . Using this solution, one can derive the initial conditions for the energy densities  $\rho_{(m)}$  and  $\rho_{(r)}$ . An exact solution of  $\Phi$  and S can also be derived on superhorizon scale [32, 35] without energy transfer

$$S_k(\xi) = S_i(k), \tag{2.28}$$

$$\Phi_k(\xi) = \Phi_i(k) \left( \frac{8}{5\xi^3} (\sqrt{1+\xi} - 1) - \frac{4}{5\xi^2} + \frac{1}{5\xi} + \frac{9}{10} \right) 
+ S_i(k) \left( \frac{16}{5\xi^3} (1 - \sqrt{1+\xi}) + \frac{8}{5\xi^2} - \frac{2}{5\xi} + \frac{1}{5} \right),$$
(2.29)

where  $\xi \equiv a/a_{\rm eq}$ , and the solution of their derivative can be directly calculated

$$S'_{k}(\xi) = 0,$$

$$\Phi'_{k}(\xi) = f(\tau)\Phi_{i}(k) \left(\frac{8}{5\xi^{3}} - \frac{1}{5\xi^{2}} + \frac{4}{5\xi^{3}\sqrt{1+\xi}} - \frac{24(\sqrt{1+\xi}-1)}{5\xi^{4}}\right)$$

$$+ f(\tau)S_{i}(k) \left(-\frac{16}{5\xi^{3}} + \frac{2}{5\xi^{2}} - \frac{8}{5\xi^{3}\sqrt{1+\xi}} - \frac{48(1-\sqrt{1+\xi})}{5\xi^{4}}\right),$$

$$f(\tau) = 2\left(\frac{1}{\tau_{*}} + \frac{\tau}{\tau^{2}}\right).$$
(2.30)

After defining the dimensionless power spectrum of Gaussian random fields  $\Phi_g$  and  $S_g^{-1}$ 

$$\langle \Phi_g(\vec{k}) \Phi_g(\vec{q}) \rangle = (2\pi)^3 \times \frac{2\pi^2}{k^3} \mathcal{P}_{\Phi_g}(k) \delta^3(\vec{k} + \vec{q})$$

$$= (2\pi)^3 \times \frac{2\pi^2}{k^3} \left( \frac{5 + 3\omega}{3 + 3\omega} \right)^2 \mathcal{P}_{\zeta_g}(k) \delta^3(\vec{k} + \vec{q}), \tag{2.32}$$

$$\langle S_g(\vec{k})S_g(\vec{q})\rangle = (2\pi)^3 \times \frac{2\pi^2}{k^3} \mathcal{P}_{S_g}(k)\delta^3(\vec{k} + \vec{q}), \qquad (2.33)$$

one can obtain the initial value of  $\Phi_i$  and  $S_i$  [51], where the equation of state parameter w is defined as  $\omega = p_{(r)}/(\rho_{(r)} + \rho_{(m)})$  and  $\zeta_g$  is the gauge invariant curvature perturbation. For the initial relative velocity  $V_{\rm rel}$ , combining Eqs. (2.24), (2.25), and the exact solutions (2.28) and (2.29) shows that during radiation-domination or matter-domination,

$$V_{\rm rel}' + 3c_s^2 \mathcal{H} V_{\rm rel} \simeq 0, \tag{2.34}$$

which leads to the regular solution  $V_{\text{rel}} = 0$ . Then, Eq. (2.13) can be applied to obtain the initial value of  $v_{(m)}$  and  $v_{(r)}$ , while Eq. (2.12) and  $S_i$  can be used to derive the initial conditions for  $\delta \rho_{(m)}$  and  $\delta \rho_{(r)}$ . The initial conditions for  $h_{ij}$  are set as usual  $(h_{ij})_i = 0$ .

## 3 Simulation results without energy transfer

As a first demonstration, we initially compare our simulation results with semi-analytical predictions in the pure isocurvature case. We subsequently generalize the initial conditions to include both adiabatic and isocurvature perturbations, and present illustrative plots highlighting their characteristic peak structures.

<sup>&</sup>lt;sup>1</sup>Generalizing to non-Gaussian fields are straightforward [51].

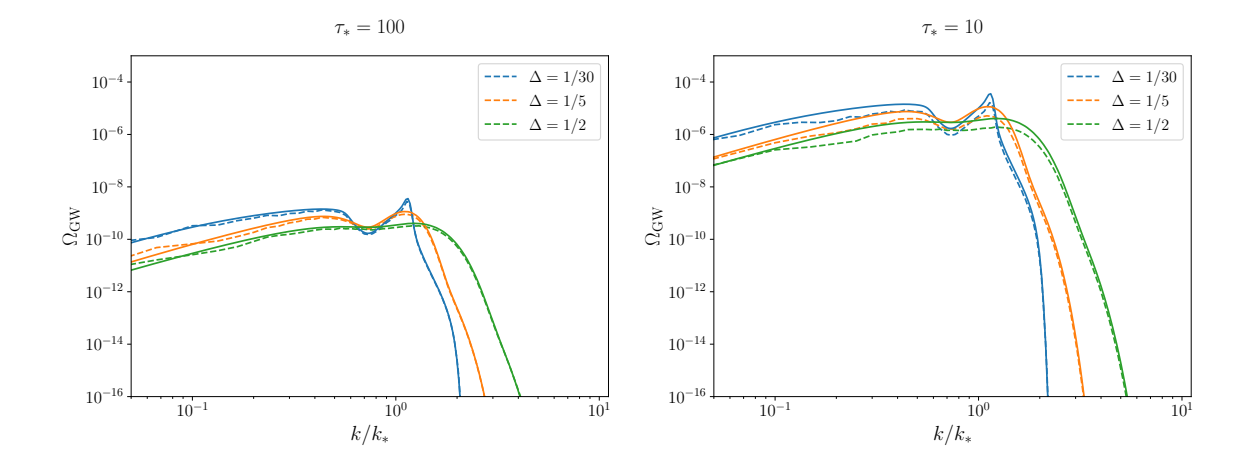


Figure 1. This figure compares the energy spectra of gravitational waves obtained via lattice simulation and semi-analytical methods. Solid lines correspond to semi-analytical results, and dashed curves represent lattice simulation outcomes. The initial amplitude of the isocurvature perturbation is B = 100, while the peak scale is chosen as  $k_* = 30$ . On the left panel, the matter-radiation equality parameter from Eq. (2.27) is set to  $\tau_* = 100$ ; on the right panel,  $\tau_* = 10$ .

# 3.1 Comparing with the semi-analytical predictions

The exact semi-analytical formulas in the isocurvature case were first derived in Ref. [50]. Provided the fluctuations enter the horizon significantly prior to matter-radiation equality, the energy spectrum of induced GWs at time  $\tau_c$  can be expressed as

$$\Omega_{\rm GW}(k,\tau_c) = \frac{2}{3} \int_0^\infty dv \int_{|1-v|}^{1+v} du \left(\frac{4v^2 - (1-u^2+v^2)^2}{4uv}\right)^2 \overline{I^2(k,\tau_c,u,v)} \mathcal{P}_S(ku) \mathcal{P}_S(kv),$$
(3.1)

where  $\overline{I^2(k,\tau_c,u,v)}$  is the kernel function, which can be found in Appendix A. For concreteness, we consider a Gaussian bump power spectrum of both curvature perturbation  $\zeta$  and isocurvature perturbation S

$$\mathcal{P}_{\zeta}(k) = A \frac{(k/k_{*1})^3}{\sqrt{2\pi}\Delta_{\text{ad}}} \exp\left[-\frac{(k/k_{*1}-1)^2}{2\Delta_{\text{ad}}^2}\right],$$
 (3.2)

$$\mathcal{P}_{S}(k) = B \frac{(k/k_{*2})^{3}}{\sqrt{2\pi}\Delta_{iso}} \exp\left[-\frac{(k/k_{*2} - 1)^{2}}{2\Delta_{iso}^{2}}\right], \tag{3.3}$$

Fig. 1 compares the energy spectra of gravitational waves from lattice simulations and semi-analytical methods, showing good agreement between each other. As noted in Ref. [50], the semi-analytical formulas remain accurate only when the characteristic modes enter the horizon well before matter-radiation equality; otherwise, modifications are required. The right panel of Fig. 1 demonstrates a suppression in the amplitude of the GW energy spectra when the peak modes enter the horizon near matter-radiation equality.

#### 3.2 The peak structures of general initial conditions

The multi-peak structure in the GW energy spectrum, originating from multi-peaked curvature perturbations, was initially investigated in Ref. [61] and later extended to scenarios with

non-Gaussianity in Ref. [62]. However, these studies focus exclusively on adiabatic perturbations. A similar multi-peak structure is also expected for isocurvature perturbations and mixed initial conditions. Considering a multi-peak Dirac delta power spectrum

$$\mathcal{P}_S(k) = \sum_{i=1}^n B_i \delta(\ln(k/k_i)). \tag{3.4}$$

Here we fix  $0 < k_1 < k_2 < ... < k_n$  without loss of generality and define  $\tilde{k}_i \equiv k/k_i$  for later convenience. One can easily obtain the multi-peak structure for the initial isocurvature perturbation

$$\Omega_{\text{GW,iso}} = \frac{2}{3} \sum_{i,j}^{n} B_i B_j \tilde{k}_i^{-1} \tilde{k}_j^{-1} \left( \frac{4\tilde{k}_i^{-2} - (1 - \tilde{k}_j^{-2} + \tilde{k}_i^{-2})^2}{4\tilde{k}_i^{-1} \tilde{k}_j^{-1}} \right)^2 \overline{I^2(k, \tau_c \to \infty, \tilde{k}_i^{-1}, \tilde{k}_j^{-1})} \\
\Theta(k_i + k_j - k) \Theta(k - |k_i - k_j|), \tag{3.5}$$

which indicates that isocurvature perturbations will exhibit a peak structure similar to that of adiabatic perturbations. Consequently, mixed initial conditions are also expected to yield an identical peak profile. The peak arises from the logarithmic pole in the kernel function  $\overline{I^2}$  and hence emerges precisely when

$$\left(\frac{k_i}{k} + \frac{k_j}{k}\right) = \sqrt{3}.\tag{3.6}$$

The number of such peaks is governed by momentum conservation, as represented by the step function in Eq. (3.5). However, in the isocurvature case, a suppression factor of the form  $(k_{\rm eq}/k_i)^4$  or  $(k_{\rm eq}/k_i)^2(k_{\rm eq}/k_j)^2$  arises. This implies that certain peaks in the mixed initial condition exhibit an explicit dependence on  $k_{\rm eq}$ .

To be specific, for the left panel of Fig. 2, we adopt  $B_1 = B_2 = 100$  in Eq. (3.4) to compute representative examples in isocurvature case; for the right panel, we choose A = 0.01 in Eq. (3.2) for adiabatic perturbation and B = 100 in Eq. (3.3) for isocurvature perturbation for numerical evaluation in mixed initial condition case.

# 4 Simulation results with energy transfer

An early PBH-dominated era provides a viable mechanism for cosmic reheating [63, 64], rendering the investigation of its observable imprints especially relevant. Additionally, certain non-topological solitons could also induce an early matter-dominated (eMD) era, potentially generating substantial gravitational wave signals [65]. In this section, we begin by examining SIGWs in the pure isocurvature case, and then extend the analysis to mixed initial conditions.

# 4.1 SIGW from eMD isocurvature

The SIGW signal induced by PBH isocurvature perturbations was initially studied and computed in Refs. [43, 44]. After their formation, PBHs are randomly distributed in space, following Poisson statistics to a very good approximation. As a result, the power spectrum of PBH density perturbations takes the form

$$\langle \delta \rho_{\rm PBH}(k) \delta \rho_{\rm PBH}(q) \rangle = \frac{4\pi}{3} \left(\frac{d}{a}\right)^3 \rho_{\rm PBH}^2 \delta(k+q),$$
 (4.1)

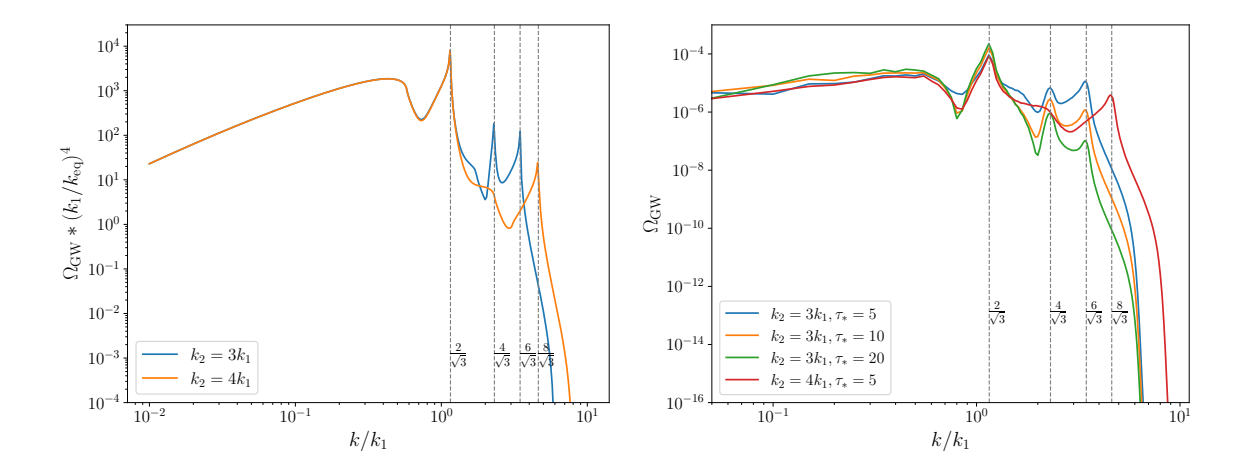


Figure 2. Peak structures for the isocurvature case (left) and the mixed initial condition case(right). Left: Semi-analytical results for the peak structure in the pure isocurvature scenario. Two representative cases are presented:  $k_2 = 3k_1$  (three distinct peaks) and  $k_2 = 4k_1$  (two peaks). Right: Lattice simulation results for the mixed initial condition, shown for different values of  $\tau_*$  and  $k_2/k_1$ . Here,  $k_1 = 20$  denotes the peak scale of the adiabatic perturbation, and  $k_2$  the peak scale of the isocurvature perturbation. The width of power spectrum has been set as  $\Delta_{\rm ad} = \Delta_{\rm iso} = 1/30$ .

where k, q are the comoving wavenumber, and d denotes the mean separation of PBHs, which can be expressed by

$$d = \frac{a}{a_f} \left( \frac{3M_{\text{PBH,f}}}{4\pi\rho_{\text{PBH,f}}} \right)^{\frac{1}{3}},\tag{4.2}$$

the subindex f means at the time of PBH formation, and  $M_{\rm PBH,f}$  is the mass of PBH. The smoothed spectrum above is valid only on coarse-grained scales larger than the comoving ultraviolet cutoff scale, which is defined as

$$k_{\rm UV} \equiv \frac{a}{d} = a_f H_f \beta^{\frac{1}{3}} \gamma^{-\frac{1}{3}},$$
 (4.3)

where  $\gamma \sim 0.2$  in the radiation-dominated (RD) era,  $H_f$  is the Hubble parameter at the time of PBH formation, and  $\beta$  denotes the fraction of PBHs at formation. Assuming that during the early radiation-dominated era (eRD), the energy density of PBHs is negligible compared to radiation at the time of PBH formation, and that initial density fluctuations on scales larger than  $k_{\rm UV}^{-1}$  can be neglected, which means  $\delta \rho_{\rm PBH,f} + \delta \rho_{r,f} = 0.2$  Therefore, the initial isocurvature perturbation is given by

$$S \simeq \frac{\delta \rho_{\rm PBH,f}}{\rho_{\rm PBH,f}},$$
 (4.4)

which leads to the dimensionless initial isocurvature power spectrum

$$\mathcal{P}_S(k) = \frac{2}{3\pi} \left(\frac{k}{k_{\text{UV}}}\right)^3 \Theta(k_{\text{UV}} - k). \tag{4.5}$$

<sup>&</sup>lt;sup>2</sup>Initial density fluctuations arise when adiabatic perturbations are considered. In contrast, isocurvature perturbations emerge following PBH formation—typically after the peak-like adiabatic perturbation has entered the horizon. Therefore, within linear perturbation theory, the adiabatic and isocurvature modes could be treated independently.

At early times following PBH formation, Hawking radiation remains negligible; hence, the initial conditions corresponding to the no-energy-transfer scenario may be adopted. The energy-transfer term can be defined as

$$aQ \equiv \rho_m a\Gamma, \tag{4.6}$$

where the decay rate is defined as

$$\Gamma \equiv -\frac{\mathrm{d}\ln M_{\mathrm{PBH}}}{\mathrm{d}t},\tag{4.7}$$

with t denoting the cosmic time. Consequently,  $\delta Q = \delta \rho_m \Gamma$ . The Hawking radiation decreases the PBH mass by [66, 67]

$$\frac{\mathrm{d}M_{\mathrm{PBH}}}{\mathrm{d}t} = -\frac{AM_{\mathrm{pl}}^4}{M_{\mathrm{PBH}}^2},\tag{4.8}$$

where  $A = 3.8\pi g(T_{\rm PBH})/480$ , and in our scenario  $g(T_{\rm PBH}) \simeq 108$ . After integration, one can obtain the PBH mass

$$M_{\rm PBH}(t) \simeq M_{\rm PBH,f} \left(1 - \frac{t}{t_{\rm eva}}\right)^{\frac{1}{3}},$$
 (4.9)

where  $t_{\text{eva}}$  describes the time of PBH evaporation, and we assume that  $t_{\text{eva}} \gg t_f$ , thus,

$$t_{\text{eva}} \simeq \frac{M_{\text{PBH,f}}^3}{3AM_{\text{pl}}^4},\tag{4.10}$$

then bringing Eq. (4.9) into Eq. (4.7), one arrives at

$$\Gamma = \frac{1}{3(t_{\text{eva}} - t)}.\tag{4.11}$$

Under the convention  $a(\tau_i) = 1$ , the conformal time roughly at matter-radiation equality,  $\tau_*$ , appeared in Eq. (2.27), is determined solely by the initial time  $\tau_i$  and the initial abundance  $\beta^3$ 

$$\tau_* = \frac{\tau_i}{\sqrt{\frac{1}{1-\beta} - 1}}.$$
(4.12)

As illustrative examples, we consider PBH masses of  $M_{\rm PBH}=10^{-4}g$  and  $2\times10^{-4}g$ , and initial abundances  $\beta=5\times10^{-2}, 10^{-2}, 5\times10^{-3}$  in our simulations<sup>4</sup>, as shown in Fig. 3. It can be seen that a larger initial abundance or a larger PBH mass leads to a steeper power-law behavior near the peak, as illustrated in Fig. 4. This behavior may originate from the different decay times of PBHs and the duration of the PBH-dominated era, an interpretation that warrants further analytical and numerical investigation in future work.

<sup>&</sup>lt;sup>3</sup>This  $\tau_*$  will only be input as a initial parameter, the real  $\tau_*$  can be obtained in the simulation.

<sup>&</sup>lt;sup>4</sup>For larger PBH masses or smaller initial abundances, the values of  $t_{\rm eva}$  or  $\tau_*$  in the simulation become very large. Simulating such cases is very challenging, which may require switching to a logarithmic time evolution scheme for the equations.

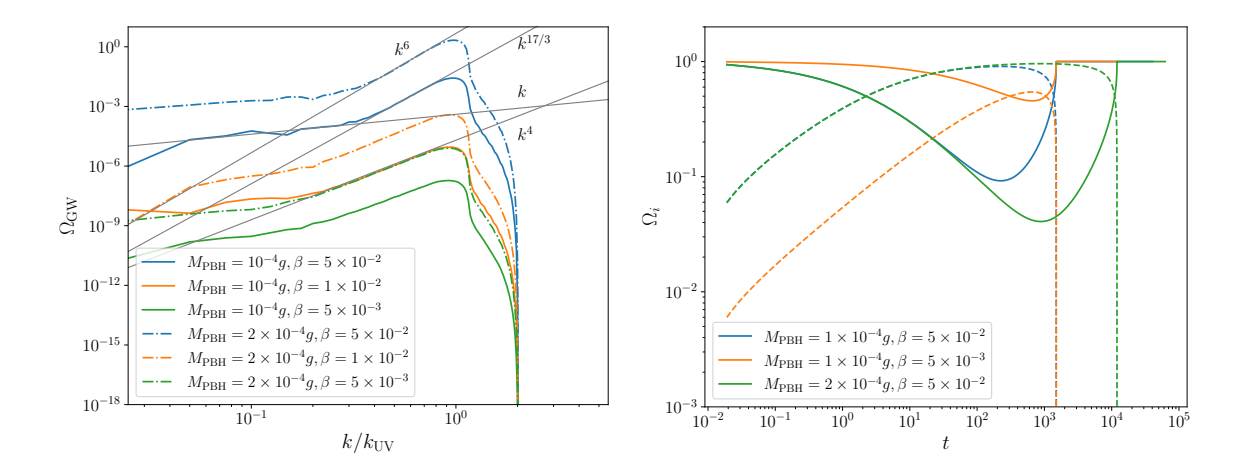


**Figure 3**. Left: The GWs energy spectra sourced by PBH isocurvature perturbations. We have set  $k_{\rm UV}=40$  in our simulations. Right: The energy density fraction  $\Omega_i=\rho_{i=m,r}/(\rho_m+\rho_r)$  of PBH and radiation. The dashed lines denote  $\Omega_m$ , while the solid line describes  $\Omega_r$ . t is the cosmic time.

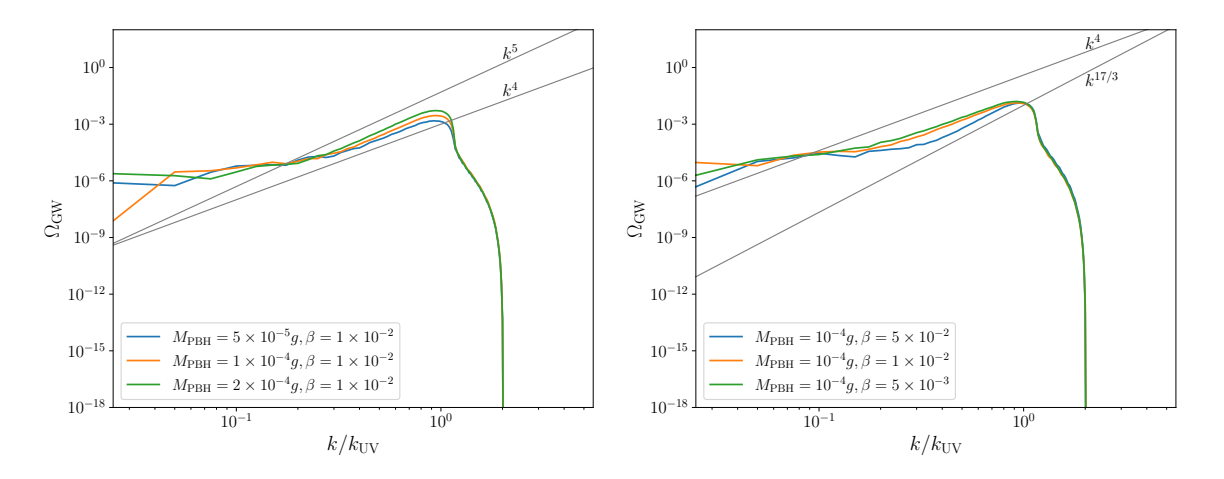


**Figure 4**. Left: The GWs energy spectra sourced by PBH isocurvature perturbations for different PBH masses. Right: The GWs energy spectra sourced by PBH isocurvature perturbations for different PBH abundances. In both figures, we have multiplied a constant to make their ultraviolet part the same.

The dynamics of non-topological solitons, such as Q-balls, are closely analogous; the primary distinction lies in their decay rates

$$\Gamma = \frac{n}{t_{\text{eva}} - t},\tag{4.13}$$

where the parameter n characterizes the decay rate for different types of solitons [68, 69], with the values n=3,1,3/5 corresponding to thin-wall Q-balls, thick-wall Q-balls, and delayed Q-balls, respectively. Figure 5 demonstrates that a slower decay rate results in both a shallower power-law index near the peak and a reduced GW amplitude. Consequently, it is imperative to derive an analytical relation between the decay rate and the GW amplitude in order to break degeneracies and distinguish among different Q-ball models and PBH populations.

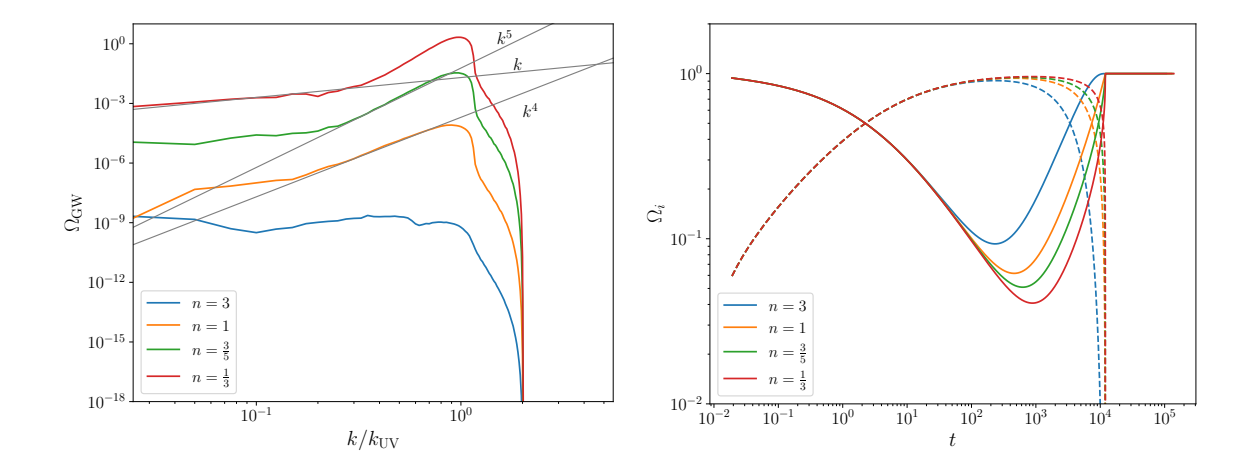


Figure 5. Left: The GWs energy spectra sourced by Q-balls isocurvature perturbations. We have set  $k_{\rm UV}=40$  in our simulations. Right: The energy density fraction  $\Omega_i=\rho_{i=m,r}/(\rho_m+\rho_r)$  of Q-balls and radiation. The dashed lines denote  $\Omega_m$ , while the solid line describes  $\Omega_r$ . t is the cosmic time. The initial abundance is set as  $\beta=5\times 10^{-2}$ .

# 4.2 SIGW from general initial conditions

A full treatment of general initial conditions is considerably more complex; here, we provide only a brief extension of the PBH-dominated case. In reality, isocurvature perturbations only emerge subsequent to PBH formation, typically well after the peak of the adiabatic perturbation has entered the horizon. Thus, one ought to initialize the adiabatic and isocurvature fluctuations at distinct times, a scenario beyond the scope of this work. Here, as an illustrative example, we simply superimpose the initial adiabatic and isocurvature contributions, while deferring the treatment of more realistic cases to future work. Assuming that PBHs are formed from a peak-like adiabatic perturbation centered at  $k_*$ , the ultraviolet cutoff scale  $k_{\rm UV}$  can be related to  $k_*$  via the identification  $k_* = \mathcal{H}_f$ 

$$k_{\rm UV} = \gamma^{-\frac{1}{3}} \beta^{\frac{1}{3}} k_*. \tag{4.14}$$

For  $\beta=10^{-2}$  and  $\gamma=0.2$ , one will obtain  $k_*\simeq 2.7k_{\rm UV}$ , which is shown in Fig. 6. As shown, the gravitational waves are initially generated by the adiabatic perturbation and are subsequently sourced by the isocurvature perturbation. The middle peak corresponds to the peak structure discussed in Subsection 3.2.

# 5 Discussion and conclusions

SIGWs represent a promising source of gravitational radiation, carrying valuable information about early-universe physics. With the advent of gravitational wave astronomy, accurate computation of the resulting GW energy spectra has become increasingly important. While numerous studies have examined SIGWs, most of them have focused primarily on adiabatic initial conditions. This study generalizes the approach of Ref. [51] to account for isocurvature initial conditions. With lattice simulations, it becomes feasible to compute SIGWs generated from mixed initial perturbations.

To validate our method, we first benchmark our simulation against semi-analytical results for pure isocurvature initial conditions [50], finding excellent agreement. However,

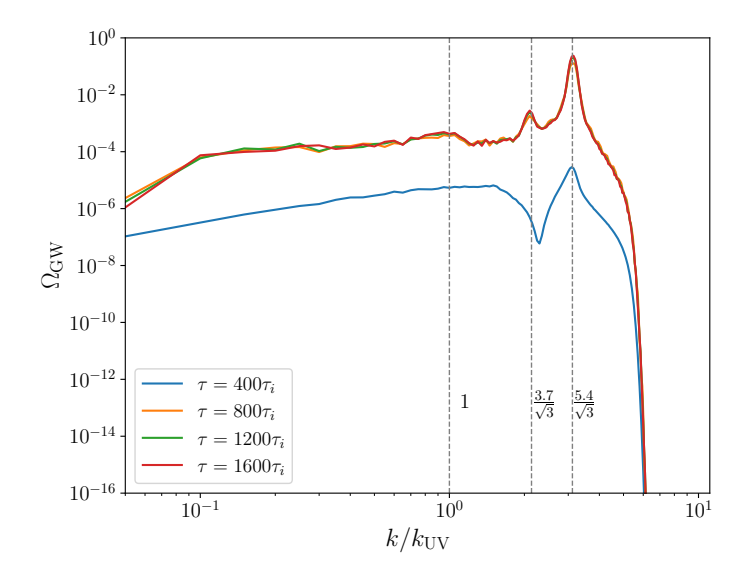


Figure 6. The GW energy spectrum sourced by the mixed initial condition at different time steps. The power spectrum of the initial adiabatic perturbation is the Gaussian bump power spectrum Eq. (3.2) with  $A = 0.01, \Delta = 1/30$  and  $k_* = 2.7k_{\rm UV} = 54$ , while the initial isocurvature power spectrum is Eq. (4.5) with  $k_{\rm UV} = 20$ .  $\tau_i$  is the initial comoving time.

when perturbations enter the horizon near the matter-radiation equality time, a discrepancy in amplitude emerges between the two approaches, suggesting the non-negligible nonlinear correction to the semi-analytical treatment. We then extend the treatment of multi-peak structures [61, 62] to mixed initial conditions. Our results show that the number and locations of the peaks remain the same as in the purely adiabatic case. The primary distinction is the presence of a scale-dependent suppression factor affecting the isocurvature contribution.

The inclusion of the energy transfer term enables a more realistic treatment of the matter-radiation system in eMD scenarios. We find that a larger initial PBH abundance or mass results in a steeper power-law spectrum near the peak. In contrast, for non-topological solitons (Q-balls), a faster decay rate (corresponding to a smaller n in Eq. (4.13)) yields a higher amplitude and a steeper slope near the peak. While the present study considers PBHs with very small masses, our results are directly relevant for guiding future analytical and numerical work. It is important to stress that our lattice simulation solves the perturbative equations of motion. Therefore, the present analysis does not account for phenomena like the nonlinear cutoff scale [52] or dynamics that lie outside the perturbative regime. Addressing this regime likely requires full numerical-relativity simulations or, at a minimum, the inclusion of the acoustic gravitational waves discussed in Refs. [70, 71].

Several important aspects warrant further investigation. As noted in Ref. [50], isocurvature perturbations are intrinsically highly non-Gaussian due to the strongly non-Gaussian nature of the density contrast  $\delta$ . It is therefore important to systematically examine non-Gaussian effects in isocurvature perturbations, as well as their influence on adiabatic perturbations that also exhibit non-Gaussianity. Future studies of the eMD scenario should address the effects of PBH accretion [72] and the effect of clustering [73, 74]. In addition, direct simulations of PBHs with larger masses are also crucial. A detailed study of these aspects will be pursued in future work.

# Acknowledgments

This work is supported by the National Key Research and Development Program of China Grant No. 2021YFC2203004, No. 2021YFA0718304, and No. 2020YFC2201501, the National Natural Science Foundation of China Grants No. 12422502, No. 12105344, No. 12235019, No. 12047503, No. 12073088, No. 11821505, No. 11991052, No. 12447101, and No. 11947302, and the China Manned Space Program Grant No. CMS-CSST-2025-A01.

# A Semi-analytical formulas in isocurvature case

In this appendix, we will mainly follow the results of Ref. [50]. Assuming the isocurvature perturbations are Gaussian, the energy spectrum of induced GWs at time  $\tau_c$  is given by

$$\Omega_{\rm GW}(k,\tau_c) = \frac{2}{3} \int_0^\infty dv \int_{|1-v|}^{1+v} du \left(\frac{4v^2 - (1-u^2+v^2)^2}{4uv}\right)^2 \overline{I^2(k,\tau_c,u,v)} \mathcal{P}_S(ku) \mathcal{P}_S(kv), \tag{A.1}$$

where the oscillation-averaged kernel function is

$$\overline{I^2(k,\tau_c,u,v)} \simeq \frac{1}{2} (I_c^2(k,\tau_c \to \infty, u, v) + I_s^2(k,\tau_c \to \infty, u, v)), \tag{A.2}$$

and the specific forms are

$$I_{c}(k,\tau_{c}\to\infty,u,v) = \frac{9}{32u^{4}v^{4}\kappa^{2}} \left\{ -3u^{2}v^{2} + (-3+u^{2})(-3+u^{2}+2v^{2}) \ln\left|1 - \frac{u^{2}}{3}\right| + (-3+v^{2})(-3+v^{2}+2u^{2}) \ln\left|1 - \frac{v^{2}}{3}\right| + (-3+v^{2})(-3+v^{2}+2u^{2}) \ln\left|1 - \frac{(u+v)^{2}}{3}\right| \right| 1 - \frac{(u-v)^{2}}{3} \right\},$$

$$I_{s}(k,\tau_{c}\to\infty,u,v) = \frac{9\pi}{32u^{4}v^{4}\kappa^{2}} \left\{ 9 - 6v^{2} - 6u^{2} + 2u^{2}v^{2} + (3-u^{2})(-3+u^{2}+2v^{2})\Theta\left(1 - \frac{u}{\sqrt{3}}\right) + (3-v^{2})(-3+v^{2}+2u^{2})\Theta\left(1 - \frac{v}{\sqrt{3}}\right) + (3-v^{2})(-3+v^{2}+2u^{2})\Theta\left(1 - \frac{v}{\sqrt{3}}\right) + \frac{1}{2}(-3+v^{2}+u^{2})^{2} \left[\Theta\left(1 - \frac{u+v}{\sqrt{3}}\right) + \Theta\left(1 + \frac{u-v}{\sqrt{3}}\right)\right] \right\},$$
(A.4)

where  $\kappa = k/k_{\rm eq}$ , and  $k_{\rm eq} = \mathcal{H}_{\rm eq}$ .

# References

[1] NANOGRAV collaboration, G. Agazie et al., The NANOGrav 15 yr Data Set: Evidence for a Gravitational-wave Background, Astrophys. J. Lett. 951 (2023) L8, [2306.16213].

- [2] EPTA, INPTA: collaboration, J. Antoniadis et al., The second data release from the European Pulsar Timing Array - III. Search for gravitational wave signals, Astron. Astrophys. 678 (2023) A50, [2306.16214].
- [3] D. J. Reardon et al., Search for an Isotropic Gravitational-wave Background with the Parkes Pulsar Timing Array, Astrophys. J. Lett. 951 (2023) L6, [2306.16215].
- [4] H. Xu et al., Searching for the Nano-Hertz Stochastic Gravitational Wave Background with the Chinese Pulsar Timing Array Data Release I, Res. Astron. Astrophys. 23 (2023) 075024, [2306.16216].
- [5] LISA collaboration, P. Amaro-Seoane et al., Laser Interferometer Space Antenna, 1702.00786.
- [6] W.-R. Hu and Y.-L. Wu, The Taiji Program in Space for gravitational wave physics and the nature of gravity, Natl. Sci. Rev. 4 (2017) 685–686.
- [7] W.-H. Ruan, Z.-K. Guo, R.-G. Cai and Y.-Z. Zhang, *Taiji program: Gravitational-wave sources*, *Int. J. Mod. Phys. A* **35** (2020) 2050075, [1807.09495].
- [8] TianQin collaboration, J. Luo et al., *TianQin: a space-borne gravitational wave detector*, Class. Quant. Grav. **33** (2016) 035010, [1512.02076].
- [9] S. Kawamura et al., The Japanese space gravitational wave antenna DECIGO, Class. Quant. Grav. 23 (2006) S125–S132.
- [10] V. Corbin and N. J. Cornish, Detecting the cosmic gravitational wave background with the big bang observer, Class. Quant. Grav. 23 (2006) 2435–2446, [gr-qc/0512039].
- [11] ET collaboration, M. Maggiore et al., Science Case for the Einstein Telescope, JCAP 03 (2020) 050, [1912.02622].
- [12] D. Reitze et al., Cosmic Explorer: The U.S. Contribution to Gravitational-Wave Astronomy beyond LIGO, Bull. Am. Astron. Soc. 51 (2019) 035, [1907.04833].
- [13] C. Caprini and D. G. Figueroa, Cosmological Backgrounds of Gravitational Waves, Class. Quant. Grav. 35 (2018) 163001, [1801.04268].
- [14] R.-G. Cai, Z. Cao, Z.-K. Guo, S.-J. Wang and T. Yang, The Gravitational-Wave Physics, Natl. Sci. Rev. 4 (2017) 687–706, [1703.00187].
- [15] L. Bian et al., The Gravitational-wave physics II: Progress, Sci. China Phys. Mech. Astron. 64 (2021) 120401, [2106.10235].
- [16] G. Domènech, Scalar Induced Gravitational Waves Review, Universe 7 (2021) 398, [2109.01398].
- [17] K. N. Ananda, C. Clarkson and D. Wands, The Cosmological gravitational wave background from primordial density perturbations, Phys. Rev. D 75 (2007) 123518, [gr-qc/0612013].
- [18] D. Baumann, P. J. Steinhardt, K. Takahashi and K. Ichiki, Gravitational Wave Spectrum Induced by Primordial Scalar Perturbations, Phys. Rev. D 76 (2007) 084019, [hep-th/0703290].
- [19] K. Kohri and T. Terada, Semianalytic calculation of gravitational wave spectrum nonlinearly induced from primordial curvature perturbations, Phys. Rev. D 97 (2018) 123532, [1804.08577].
- [20] J. R. Espinosa, D. Racco and A. Riotto, A Cosmological Signature of the SM Higgs Instability: Gravitational Waves, JCAP 09 (2018) 012, [1804.07732].
- [21] T. Terada, Semianalytic calculation of the gravitational wave spectrum induced by curvature perturbations, 2509.18694.
- [22] R.-g. Cai, S. Pi and M. Sasaki, *Gravitational Waves Induced by non-Gaussian Scalar Perturbations*, *Phys. Rev. Lett.* **122** (2019) 201101, [1810.11000].
- [23] C. Unal, Imprints of Primordial Non-Gaussianity on Gravitational Wave Spectrum, Phys. Rev. D 99 (2019) 041301, [1811.09151].

- [24] P. Adshead, K. D. Lozanov and Z. J. Weiner, Non-Gaussianity and the induced gravitational wave background, JCAP 10 (2021) 080, [2105.01659].
- [25] K. Inomata and T. Nakama, Gravitational waves induced by scalar perturbations as probes of the small-scale primordial spectrum, Phys. Rev. D 99 (2019) 043511, [1812.00674].
- [26] R.-G. Cai, S.-J. Wang, Z.-Y. Yuwen and X.-X. Zeng, Anisotropies of cosmological gravitational wave backgrounds in non-flat spacetime, JCAP 01 (2025) 011, [2410.17721].
- [27] PLANCK collaboration, Y. Akrami et al., Planck 2018 results. X. Constraints on inflation, Astron. Astrophys. 641 (2020) A10, [1807.06211].
- [28] WMAP collaboration, C. L. Bennett et al., First year Wilkinson Microwave Anisotropy Probe (WMAP) observations: Preliminary maps and basic results, Astrophys. J. Suppl. 148 (2003) 1–27, [astro-ph/0302207].
- [29] Planck collaboration, N. Aghanim et al., Planck 2018 results. VI. Cosmological parameters, Astron. Astrophys. 641 (2020) A6, [1807.06209].
- [30] H. Kodama and M. Sasaki, Cosmological Perturbation Theory, Prog. Theor. Phys. Suppl. 78 (1984) 1–166.
- [31] H. Kodama and M. Sasaki, Evolution of Isocurvature Perturbations. 1. Photon Baryon Universe, Int. J. Mod. Phys. A 1 (1986) 265.
- [32] H. Kodama and M. Sasaki, Evolution of Isocurvature Perturbations. 2. Radiation Dust Universe, Int. J. Mod. Phys. A 2 (1987) 491.
- [33] D. Langlois, Isocurvature cosmological perturbations and the CMB, Comptes Rendus Physique 4 (2003) 953–959.
- [34] M. Bucher, K. Moodley and N. Turok, The General primordial cosmic perturbation, Phys. Rev. D 62 (2000) 083508, [astro-ph/9904231].
- [35] G. Domènech, Cosmological gravitational waves from isocurvature fluctuations, AAPPS Bull. 34 (2024) 4, [2311.02065].
- [36] D. J. H. Chung and A. Upadhye, Search for strongly blue axion isocurvature, Phys. Rev. D 98 (2018) 023525, [1711.06736].
- [37] D. J. H. Chung and S. C. Tadepalli, Analytic treatment of underdamped axionic blue isocurvature perturbations, Phys. Rev. D 105 (2022) 123511, [2110.02272].
- [38] D. H. Lyth and D. Wands, Generating the curvature perturbation without an inflaton, Phys. Lett. B **524** (2002) 5–14, [hep-ph/0110002].
- [39] D. Polarski and A. A. Starobinsky, *Isocurvature perturbations in multiple inflationary models*, *Phys. Rev. D* **50** (1994) 6123–6129, [astro-ph/9404061].
- [40] A. D. Linde, Generation of Isothermal Density Perturbations in the Inflationary Universe, Phys. Lett. B 158 (1985) 375–380.
- [41] M. R. Buckley, P. Du, N. Fernandez and M. J. Weikert, Dark radiation isocurvature from cosmological phase transitions, JCAP 07 (2024) 031, [2402.13309].
- [42] D. Inman and Y. Ali-Haïmoud, Early structure formation in primordial black hole cosmologies, Phys. Rev. D 100 (2019) 083528, [1907.08129].
- [43] T. Papanikolaou, V. Vennin and D. Langlois, Gravitational waves from a universe filled with primordial black holes, JCAP 03 (2021) 053, [2010.11573].
- [44] G. Domènech, C. Lin and M. Sasaki, Gravitational wave constraints on the primordial black hole dominated early universe, JCAP 04 (2021) 062, [2012.08151].
- [45] G. Domènech, V. Takhistov and M. Sasaki, Exploring evaporating primordial black holes with gravitational waves, Phys. Lett. B 823 (2021) 136722, [2105.06816].

- [46] G. Domènech and J. Tränkle, From formation to evaporation: Induced gravitational wave probes of the primordial black hole reheating scenario, Phys. Rev. D 111 (2025) 063528, [2409.12125].
- [47] S. Balaji, G. Domènech, G. Franciolini, A. Ganz and J. Tränkle, Probing modified Hawking evaporation with gravitational waves from the primordial black hole dominated universe, JCAP 11 (2024) 026, [2403.14309].
- [48] K. D. Lozanov, M. Sasaki and V. Takhistov, *Universal gravitational wave signatures of cosmological solitons*, *JCAP* **01** (2025) 094, [2304.06709].
- [49] K. D. Lozanov, M. Sasaki and V. Takhistov, Universal gravitational waves from interacting and clustered solitons, Phys. Lett. B 848 (2024) 138392, [2309.14193].
- [50] G. Domènech, S. Passaglia and S. Renaux-Petel, Gravitational waves from dark matter isocurvature, JCAP 03 (2022) 023, [2112.10163].
- [51] X.-X. Zeng, Z. Ning, R.-G. Cai and S.-J. Wang, Scalar-induced gravitational waves with non-Gaussianity up to all orders, 2508.10812.
- [52] H. Assadullahi and D. Wands, Gravitational waves from an early matter era, Phys. Rev. D 79 (2009) 083511, [0901.0989].
- [53] K. Inomata, K. Kohri, T. Nakama and T. Terada, Enhancement of Gravitational Waves Induced by Scalar Perturbations due to a Sudden Transition from an Early Matter Era to the Radiation Era, Phys. Rev. D 100 (2019) 043532, [1904.12879].
- [54] K. Inomata, M. Kawasaki, K. Mukaida, T. Terada and T. T. Yanagida, Gravitational Wave Production right after a Primordial Black Hole Evaporation, Phys. Rev. D 101 (2020) 123533, [2003.10455].
- [55] K. Inomata, K. Kohri, T. Nakama and T. Terada, Gravitational Waves Induced by Scalar Perturbations during a Gradual Transition from an Early Matter Era to the Radiation Era, JCAP 10 (2019) 071, [1904.12878].
- [56] M. Pearce, L. Pearce, G. White and C. Balazs, Gravitational wave signals from early matter domination: interpolating between fast and slow transitions, JCAP 06 (2024) 021, [2311.12340].
- [57] Z.-M. Zeng, C.-J. Fang and Z.-K. Guo, Critical behavior and ultraviolet scaling of induced gravitational waves from an early matter-dominated era, 2504.01397.
- [58] G. Domènech and J. Tränkle, Gravitational waves induced by matter isocurvature in general cosmologies, 2509.02122.
- [59] M. Maggiore, Gravitational wave experiments and early universe cosmology, Phys. Rept. **331** (2000) 283–367, [gr-qc/9909001].
- [60] C. Pitrou, X. Roy and O. Umeh, xPand: An algorithm for perturbing homogeneous cosmologies, Class. Quant. Grav. 30 (2013) 165002, [1302.6174].
- [61] R.-G. Cai, S. Pi, S.-J. Wang and X.-Y. Yang, Resonant multiple peaks in the induced gravitational waves, JCAP 05 (2019) 013, [1901.10152].
- [62] X.-X. Zeng, R.-G. Cai and S.-J. Wang, Multiple peaks in gravitational waves induced from primordial curvature perturbations with non-Gaussianity, JCAP 10 (2024) 045, [2406.05034].
- [63] J. E. Lidsey, T. Matos and L. A. Urena-Lopez, The Inflaton field as selfinteracting dark matter in the brane world scenario, Phys. Rev. D 66 (2002) 023514, [astro-ph/0111292].
- [64] J. C. Hidalgo, L. A. Urena-Lopez and A. R. Liddle, *Unification models with reheating via Primordial Black Holes, Phys. Rev. D* 85 (2012) 044055, [1107.5669].
- [65] G. White, L. Pearce, D. Vagie and A. Kusenko, Detectable Gravitational Wave Signals from Affleck-Dine Baryogenesis, Phys. Rev. Lett. 127 (2021) 181601, [2105.11655].

- [66] H. I. Kim, C. H. Lee and J. H. MacGibbon, Diffuse gamma-ray background and primordial black hole constraints on the spectral index of density fluctuations, Phys. Rev. D 59 (1999) 063004, [astro-ph/9901030].
- [67] D. Hooper, G. Krnjaic and S. D. McDermott, Dark Radiation and Superheavy Dark Matter from Black Hole Domination, JHEP 08 (2019) 001, [1905.01301].
- [68] M. Pearce, L. Pearce, G. White and C. Balázs, *Using Gravitational Wave Signals to Disentangle Early Matter Dominated Epochs*, 2503.03101.
- [69] T. Multamaki and I. Vilja, Analytical and numerical properties of Q balls, Nucl. Phys. B 574 (2000) 130–152, [hep-ph/9908446].
- [70] X.-X. Zeng, Z. Ning, Z.-Y. Yuwen, S.-J. Wang, H. Deng and R.-G. Cai, *Relic gravitational waves from primordial gravitational collapses*, 2504.11275.
- [71] Z. Ning, X.-X. Zeng, Z.-Y. Yuwen, S.-J. Wang, H. Deng and R.-G. Cai, Sound waves from primordial black hole formations, 2504.12243.
- [72] R. Allahverdi, J. B. Dent, N. P. D. Loc and T. Xu, Gravitational wave signatures of primordial black hole accretion during early matter domination, 2505.21885.
- [73] X.-C. He, Y.-F. Cai, X.-H. Ma, T. Papanikolaou, E. N. Saridakis and M. Sasaki, Gravitational waves from primordial black hole isocurvature: the effect of non-Gaussianities, JCAP 12 (2024) 039, [2409.11333].
- [74] T. Papanikolaou, X.-C. He, X.-H. Ma, Y.-F. Cai, E. N. Saridakis and M. Sasaki, New probe of non-Gaussianities with primordial black hole induced gravitational waves, Phys. Lett. B 857 (2024) 138997, [2403.00660].